Effect of Aza Substitution on the Photophysical and Electrochemical Properties of Porphycenes: Characterization of the Near-IR-Absorbing Photosensitizers 2,7,12,17-Tetrakis(*p*-substituted phenyl)-3,6,13,16-tetraazaporphycenes

Noemí Rubio, David Sánchez-García, Ana Jiménez-Banzo, Óscar Rey, José I. Borrell, Jordi Teixidó, and Santi Nonell*

Grup d'Enginyeria Molecular, Institut Químic de Sarrià, Universitat Ramon Llull, Via Augusta 390, 08017 Barcelona, Spain

Received: November 9, 2005; In Final Form: December 22, 2005

The need for new photodynamic-therapy photosensitizers has stimulated the search of new families of compounds absorbing strongly in the 700−900 nm range, the region where tissue is most transparent to radiation capable to induce the photodynamic effect. Using computational chemistry techniques, 3,6,13,16-tetraazaporphycenes were previously identified as interesting target candidates. This work reports on the photophysical and electrochemical properties of selected members of this new family of macrocycles. Compared to porphycenes, the tetra-aza counterparts show stronger absorption in the near-infrared, lower-lying singlet and triplet excited states, and substantially larger internal conversion quantum yield ($\Phi_{IC} = 0.93$). Energy transfer to oxygen is observed, which results in the formation of the cytotoxic species singlet oxygen. The process is found to be reversible, consistent with a triplet-energy value close to that of singlet oxygen.

1. Introduction

Photodynamic therapy (PDT) has emerged as an attractive treatment of cancer based on the combined action of a photosensitizing drug (referred to as the photosensitizer), red to near-infrared radiation, and molecular oxygen to induce a cytotoxic effect through the generation of highly reactive oxygen species (ROS), particularly singlet oxygen, $O_2(^1\Delta_g)$. Several families of compounds are currently being investigated as potential PDT drugs, most of them based on structural variations of the porphyrin macrocycle.[1−10]

One of the goals of these developments is to improve the light absorption properties of the drugs, which should ideally absorb in the 700−900 nm range, where biological tissues are most transparent,[4] and possess large absorption coefficients. Porphyrins currently in use for PDT absorb below 650 nm and have absorption coefficients not exceeding 5×10^3 $M^{-1}\cdot cm^{-1}$.

Red shifts in the absorption spectrum can be achieved by enlarging the size of the aromatic macrocycle,[11−17] by suitable peripheral functionalization,[18−20] or by introducing heteroatoms in the macrocycle core, particularly nitrogens.[12,21−26] In designing such modifications, one must keep in mind that the wavelength of the lowest-energy absorption band should not exceed an upper-limit value dictated by a number of factors:[27] (i) water, the main constituent in living cells, absorbs strongly in the near-infrared thus increasingly acting as an inner filter;[28] (ii) near-infrared photosensitizers are more sensitive to oxidation and thus to photobleaching owing to the higher electron availability,[9] and (iii) the triplet excited state of a photosensitizer must lie above the energy level of singlet oxygen (94.2 $kJ\cdot mol^{-1}$) for effective energy transfer to this cytotoxic species.[29] Assuming a typical singlet−triplet splitting of ca. 40 $kJ\cdot mol^{-1}$,[27] ground-state absorption should be below 900 nm.

CHART 1: Structures of Porphyrins, Chlorins, Porphycenes and Azaporphycenes

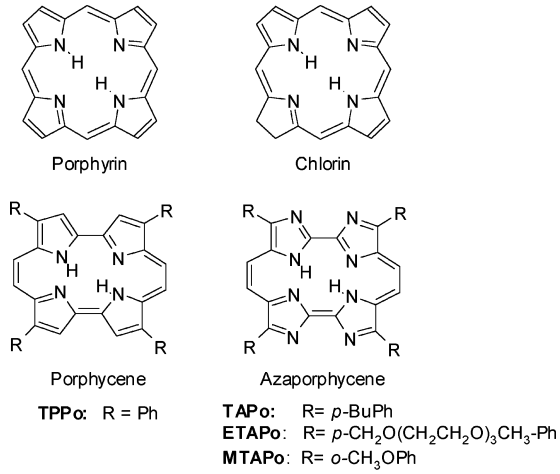

Similarly, the absorption coefficient of the sensitizer can be increased by reducing its symmetry, thereby lifting the prohibition on the absorption transitions. Chlorins,[3,30] where one of the pyrrole rings is reduced, and porphycenes,[31,32] lower-symmetry isomers of porphyrins, are very good examples of this symmetry effect, with absorption coefficients 1 order of magnitude larger than those of porphyrins (Chart 1). Hyperchromism at the lowest-energy bands can also be achieved by aza substitution in the tetrapyrrole skeleton.[21−23,25]

On the basis of the above rationale, we set out to develop aryl-substituted porphycene photosensitizers for PDT. Thus, tetraphenylporphycene (TPPo) was initially developed, which absorbs at 659 nm with absorption coefficient 5×10^4 $M^{-1}\cdot cm^{-1}$.[20,33] For comparison, alkyl-substituted porphycenes absorb at ca. 630 nm and show lower absorption coefficients (3×10^4 $M^{-1}\cdot cm^{-1}$).[32] TPPo and its palladium complex show excellent photosensitizing properties against a wide range of

* To whom correspondence should be addressed. E-mail: s.nonell@iqs.url.edu. Tel: (+34) 93 267 2000. Fax: (+34) 93 205 6266.

10.1021/jp056494+ CCC: $33.50
Published on Web 02/23/2006

cancer cell lines at concentrations substantially lower than those of porphyrins.[34−37]

The batho- and hyperchromic effects brought about by aza susbtitution in porphyrins prompted us to explore whether such effects would also occur in porphycenes. Nussbaumer et al. had previously shown that the introduction of nitrogen atoms in the porphycene analogue 21,23-dithiaporphycene causes a bathochromic shift of 23−59 nm relative to that of 21,23-dithiaporphycene.[26] Hence, a systematic computational study on the effects of aza substitution on the absorption properties of arylporphycenes was undertaken and we identified 2,7,12,17-tetraaryl-3,6,13,16-tetraazaporphycenes as the most interesting candidates for synthesis.[38] Indeed, the first candidate synthesized, 2,7,12,17-tetrakis(4-butylphenyl)-3,6,13,16-tetraazaporphycene (TAPo, Chart 1), showed a bathochromic shift of 101 nm relative to 2,7,12,17-tetraphenylporphycene, actually 20 nm larger than predicted.

It was thus of interest to study whether and how aza substitution would modify the photophysical and photosensitizing properties of porphycenes. The results of such studies are reported herein and provide clues for the further development of porphycene photosensitizers with fine-tuned properties.

2. Experimental Section

Chemicals. TAPo was synthesized as previously described.[38] The synthesis of 2,7,12,17-tetrakis(2-methoxyphenyl)-3,6,13,16-tetraazaporphycene (MTAPo, Chart 1) and 2,7,12,17-tetrakis(4-{[2-[2-(2-methoxyethoxy)ethoxy]ethoxy]methyl}phenyl)-3,6,13,16-tetraazaporphycene (ETAPo, Chart 1) is described in the Supporting Information. Benzene, benzene-d_6, toluene, dimethyl sulfoxide (DMSO), and dichloromethane from Solvents Documentation Syntheses (SDS), as well as tetrahydrofuran (THF) and ethyl iodide from Sigma-Aldrich were of the highest purity available and were used as received. Benzonitrile (Fluka, 99.9%) was dried over 4 Å molecular sieves. Indocyanine green and β-carotene (Car) were purchased from Sigma-Aldrich and were used as received. Phenalenone was purchased from Sigma-Aldrich and was recrystallized from EtOH. Electrochemical grade tetrabutylammonium hexafluorophosphate ($TBAPF_6$) was purchased from Fluka. C_{60} was purchased from Texas Fullerenes. Argon (>99.9%) and oxygen (>99.9%) were from Abelló-Linde.

Photophysical Measurements. Unless otherwise stated, all photophysical measurements were carried out in toluene solutions. Absorption spectra were recorded on a Varian Cary 4E spectrophotometer. Fluorescence spectra were recorded on a Jobin Yvon-Spex Fluoromax-2 spectrofluometer. Fluorescence decays were recorded with a time-correlated single photon counting system (Fluotime 200, PicoQuant GmbH, Berlin, Germany) equipped with a red-sensitive photomultiplier. A 654-nm picosecond diode laser working at 10 MHz repetition rate was used for excitation with counting frequency below 1%. The system was customized to detect near-IR phosphorescence using a Q-switched diode-pumped Nd:YAG laser (FTSS 355-Q, Crystal Laser, Berlin, Germany; 14 kHz repetition frequency, 3.8 mW quasi-CW power at 355 nm) for excitation, a near-IR sensitive photomultiplier tube with 300 ps TTS (H9170-45, Hamamatsu Photonics Deutschland GmbH, Herrsching, Germany) for detection, and a Becker&Hickl (Berlin, Germany) MSA 300 board for photon counting. The PicoQuant FluoFit software was used for data analysis.

Triplet−triplet absorption was studied with a nanosecond flash photolysis system made up of a Q-switched Nd:YAG laser (Surelite I-10, Continuum) coupled to an OPO laser (SL OPO, Continuum) for excitation (5 ns pulse width). Absorbance changes were monitored at 90° by an analyzing beam produced by a Xe lamp (PTI, 75W) in combination with a monochromator (PTI) and a red-sensitive photomultiplier (R928, Hasmamatsu).[20] Production and quenching of singlet oxygen were assessed by time-resolved near-IR emission spectroscopy (TRNIR) using a germanium detector (North Coast EO-817P).[39]

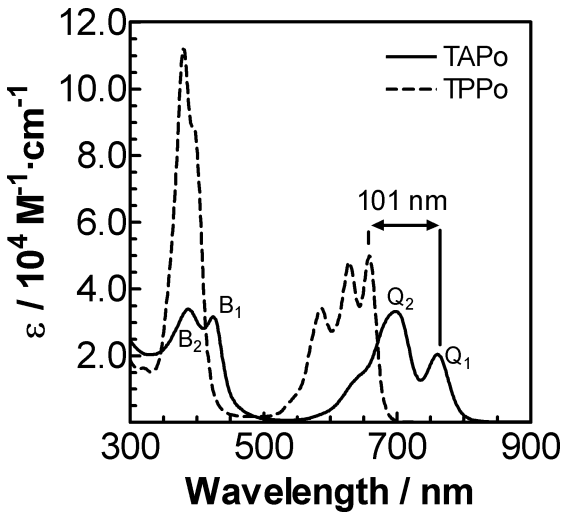

Figure 1. Absorption spectrum of TAPo in toluene. The spectrum of TPPo is provided for comparison. No changes are observed in the range 0.5−200 μM.

Absorption coefficients were determined from Beer−Lambert plots. The fluorescence quantum yield was determined by comparison of the areas under the emission curves for absorbance-matched solutions of TAPo and a reference, after correcting for the refractive index of the solvent ($\lambda_{exc} = 720$ nm). Indocyanine green (ICG) was used as reference with $\Phi_F = 0.13$ in DMSO.[40] The absorbance of the solutions was kept below 0.05 to prevent inner-filter effects. The quantum yield of singlet oxygen production, Φ_Δ, was determined by the comparative method from the amplitude of the singlet oxygen phosphorescence signal, $S(0)$,[39] using phenalenone (PN) as standard with $\Phi_\Delta = 0.94$ in benzene and benzene-d_6.[41] This method compares the amplitudes of the singlet oxygen signals obtained from both the reference and the sample at the same excitation wavelength, in this case $\lambda_{exc} = 416$ nm, at the same intensity and with samples of the same absorbance at the excitation wavelength.

Electrochemical Measurements. The redox potentials of TAPo were determined by cyclic voltammetry. A cylindrical cell was used with a 0.093 cm^2 platinum sphere as the working electrode, a platinum wire as the counter-electrode, and a Ag/AgCl 3.5 M as the reference electrode. A salt bridge containing $TBAPF_6$ 0.5 M was inserted between the working and the reference electrode compartments. The voltammograms were recorded in nitrogen-saturated dried benzonitrile using 0.1 M $TBAPF_6$ as supporting electrolyte, with sweep speeds ranging from 50 to 200 mV/s.

3. Results

Absorption and Fluorescence Data. The absorption spectrum of TAPo shows distinct absorption bands in the red, with the lowest-energy maximum at 760 nm ($\epsilon = 2.04 \times 10^4$ $M^{-1}\cdot cm^{-1}$), 101 nm red shifted relative to TPPo[20] (Figure 1). The Beer−Lambert plots are linear over at least 3 orders of magnitude in concentration, thus ruling out the presence of dimers or higher aggregates. The absorption spectrum follows the pattern of porphycenes, which in turn can be described using

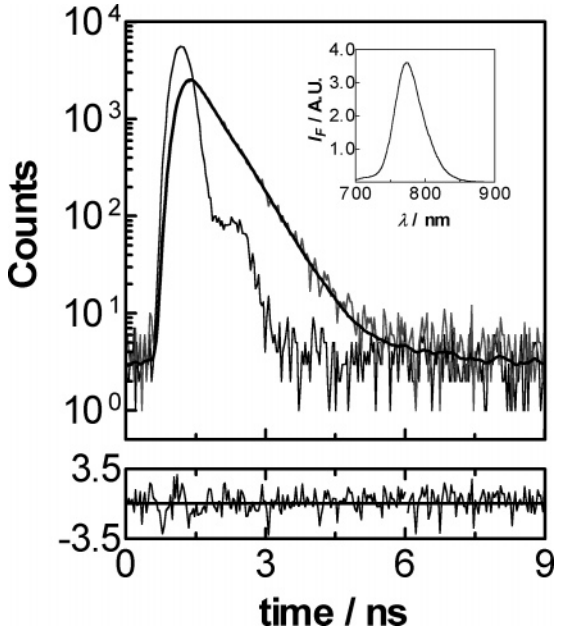

Figure 2. Fluorescence decay of TAPo in toluene ($\lambda_{exc} = 654$ nm; $\lambda_{obs} = 777$ nm). The upper panel shows the fluorescence decay, the instrument response function, and the fit to a monoexponential function convoluted with the instrument response function. The bottom panel shows the error distribution of the fit, for which $\chi^2 = 1.015$. Inset: fluorescence spectrum of TAPo in toluene ($\lambda_{exc} = 654$ nm).

the nomenclature of porphyrins: the red part of the spectrum is the Q region, formed by two electronic transitions termed Q_1 and Q_2, the latter showing vibrational structure. The blue part is the Soret region, in turn showing two transitions termed B_1 and B_2.[42] The oscillator strength of the Soret transitions is distinctly smaller than for TPPo, a situation that is reminiscent of that observed in phthalocyanines.[43] MTAPo shows a similar absorption spectrum than TAPo although slightly blue shifted (11 nm; see Supporting Information). The spectrum of ETAPo in water shows that it is aggregated to a large extent. Because aggregation of photosensitizers usually deteriorates their photophysical properties and reduces their effectiveness as PDT photosensitizers,[27] studies on ETAPo were discontinued at this point as this compound was primarily synthesized for its use in aqueous solutions. In nonaqueous solvents such as methanol, the properties are essentially identical to those of TAPo.

The fluorescence emission spectrum shows a single band with maximum at 777 nm, independent of the excitation wavelength (Figure 2, inset). The fluorescence quantum yield is $\Phi_F = 0.03 \pm 0.006$ (0.02 ± 0.004 for MTAPo), ca. one-fifth the value for TPPo ($\Phi_F = 0.15$).[20] The singlet lifetime is $\tau_S = 0.52$ ns (Figure 2) and is not affected by oxygen (0.34 ns is observed for MTAPo). Combining the Φ_F and τ_S values, the radiative rate constant is readily calculated as $k_F = \Phi_F/\tau_S = 5.8 \times 10^7$ s^{-1}, ca. 2-fold larger than that of TPPo, 3.1×10^7 s^{-1}.[20] This confirms the expectation that aza substitution in porphycenes brings about a hyperchromic effect.

From the crossing point between the normalized absorption and emission spectra the singlet energy of TAPo is placed at $E_S = 156$ kJ·mol^{-1}, i.e., 25 kJ·mol^{-1} lower than that of TPPo.[20] The value for MTAPo is very similar, 157 kJ·mol^{-1}.

Triplet-State Properties. Photoexcitation of TAPo leads to the formation of its triplet state, which shows an absorption maximum at 524 nm and lives 42 ± 3 μs in argon-saturated toluene solutions (Figure 3). It is quenched by oxygen (Figure 4) with a rate constant of $k_q^{O_2} = (1.7 \pm 0.2) \times 10^9$ M^{-1}·s^{-1} (see Supporting Information), a value ca. 40% lower than that

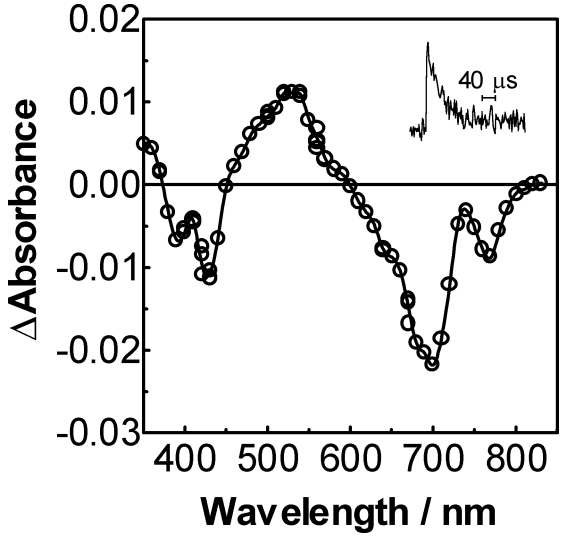

Figure 3. Triplet-minus-singlet absorption spectrum of TAPo in argon-saturated toluene. Inset: monoexponential decay for TAPo ($\lambda_{exc} = 668$ nm; $\lambda_{obs} = 524$ nm).

observed for related macrocycles (e.g., $k_q^{O_2} = 2.9 \times 10^9$ M^{-1}·s^{-1} for TPPo).[20] Under air-saturation conditions, but not under argon nor under oxygen, the transient shows biexponential decay. These observations suggest that the triplet level of TAPo is close to that of singlet oxygen (94.2 kJ·mol^{-1}).[44−47]

Indeed, using a highly sensitive near-IR photomultiplier, we were able to record the phosphorescence spectrum of TAPo in THF−ethyl iodide (4:3) glass at 77 K, which shows a maximum at 1240 nm (Figure 5). This sets its triplet-energy level at 98 ± 2 kJ·mol^{-1}, well below ^{3}TPPo (124 kJ·mol^{-1})[20] and slightly above singlet oxygen (94 kJ·mol^{-1}), as expected.

Singlet Oxygen Formation. Consistent with a triplet-energy value slightly above that of $O_2(^1\Delta_g)$ and with the oxygen ability to quench its triplet state, TAPo is able to photosensitize the production of $O_2(^1\Delta_g)$ (Figure 6). A number of particular features are noteworthy: (i) The quantum yield for singlet oxygen formation, Φ_Δ, depends on the concentration of molecular oxygen in the media. Thus, $\Phi_\Delta = 0.023 \pm 0.003$ in air-saturated benzene and perdeuterated benzene and increases to 0.043 ± 0.003 as the solvent is saturated with oxygen. The value for MTAPo under air is 0.034 ± 0.003. (ii) The decay part of the signal shows two components: a fast one, which is generally ascribed to the tail of sensitizer fluorescence/phosphorescence, and a slowest one, assigned to $O_2(^1\Delta_g)$, which obeys first-order kinetics. (iii) The $O_2(^1\Delta_g)$ lifetime, τ_Δ, is clearly shorter relative to that observed with PN as photosensitizer. This is particularly obvious in perdeuterated benzene. In fact, the effect of TAPo on the rate of $O_2(^1\Delta_g)$ decay can be described by

$$1/\tau_\Delta = 1/\tau_\Delta^0 + k_q^{TAPo}[TAPo] \quad (1)$$

where τ_Δ^0 is the singlet oxygen lifetime at zero TAPo concentration. TAPo acts thus as a $O_2(^1\Delta_g)$ quencher with rate constant $k_q^{TAPo} = (3.5 \pm 0.8) \times 10^8$ M^{-1}·s^{-1} (Figure 6, inset).

Triplet-Energy Transfer to β-Carotene. To confirm the triplet-energy value, energy-transfer experiments to β−carotene (Car) were carried out. Likewise, the absorbance of ^{3}Car in absorbance-matched solutions of TAPo and C_{60} was compared to determine the triplet quantum yield. Thus, in the presence of Car, the rate of decay of ^{3}TAPo increased and the concomitant formation of ^{3}Car with the same rate was readily observed (Figure 7). It is noteworthy that the lifetime of ^{3}Car showed a

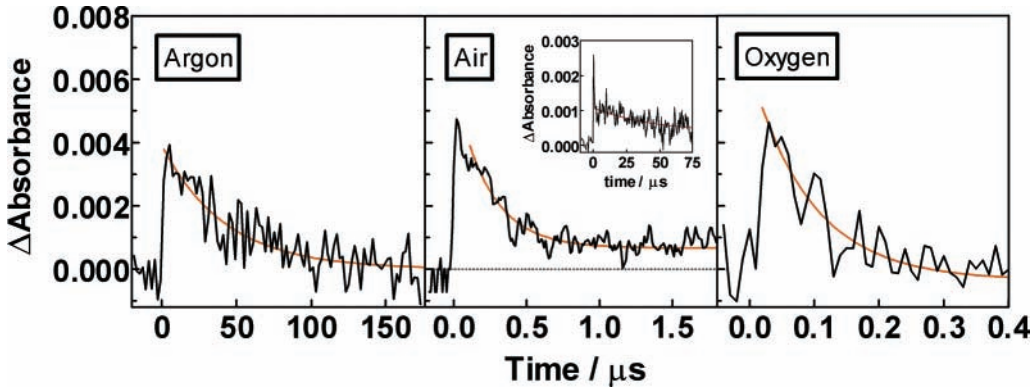

Figure 4. Transient absorption of triplet TAPo in argon-, air-, and oxygen-saturated toluene (λ_{exc} = 668 nm; λ_{obs} = 524 nm; [TAPo] = 20 μM). Note that the signal does not return to zero in the air-saturated sample but a second, slower-decaying component with lifetime 32 μs can be seen (see inset).

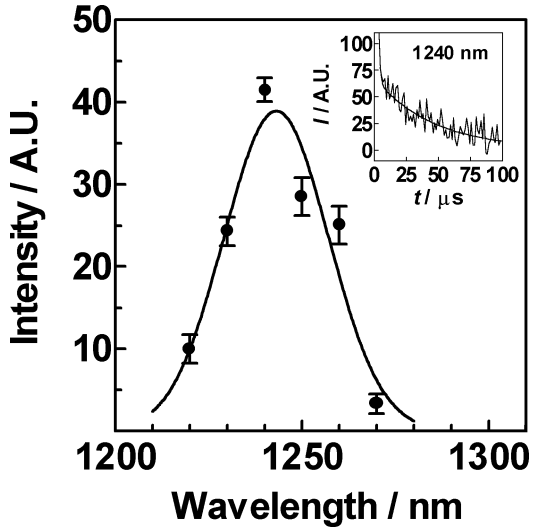

Figure 5. Near-IR phosphorescence spectrum of TAPo at 77 K in a THF−ethyl iodide (4:3) glass (λ_{exc} = 355 nm). Inset: phosphorescence decay at 1240 nm.

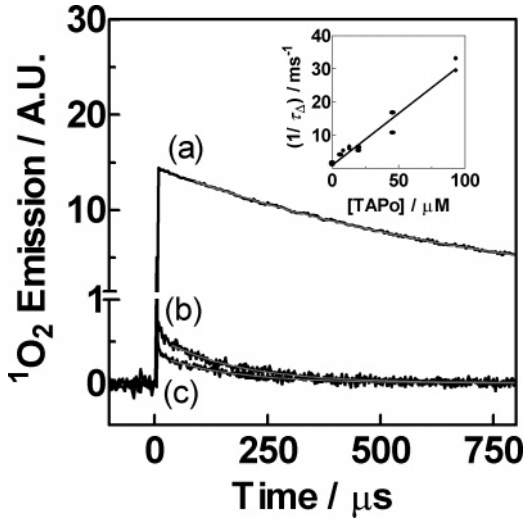

Figure 6. Singlet oxygen phosphorescence at 1270 nm in perdeuterated-benzene sensitized by (a) PN in air- and O_2-saturated solutions, and TAPo 90 μM in (b) O_2-saturated and (c) air-saturated solutions; λ_{exc} = 416 nm. The PN and TAPo solutions were absorbance-matched. Inset: reciprocal singlet oxygen lifetime as a function of TAPo concentration.

marked dependence on the ground-state Car concentration (5.3 ± 0.2 μs at 180 and 200 μM Car, but 8.0 ± 0.7 μs at 90 μM Car).

From the plot of the rate constant for ^{3}Car formation vs [Car], the bimolecular rate constant for energy transfer from ^{3}TAPo to Car is calculated using the relationship $k_1 = 1/\tau_1 = k_0 + k_{et}$[Car], where k_0 is an empirical parameter (see Discussion). Linear regression yields $k_{et} = (2.2 \pm 0.2) \times 10^9$ M^{-1}·s^{-1} and $k_0 = (6.5 \pm 0.4) \times 10^4$ s^{-1}. (Figure 8). Interestingly, k_0 is 3-fold larger than the rate constant for ^{3}TAPo decay at [Car] = 0, $k_{TAPo} = 2.2 \times 10^4$ s^{-1}.

When the same experiment was done using C_{60} as energy donor (E_T = 147 kJ·mol^{-1}, well above that of ^{3}Car),[48] Car quenched the $^3C_{60}$ with rate constant ca. 3-fold larger, $k_{et}^{C60} = 5.6 \times 10^9$ M^{-1}·s^{-1} (see Supporting Information) and the lifetime of the ensuing ^{3}Car was 5.3 ± 0.2 μs at all Car concentrations (Figure 9). As shown in the Discussion, the relative transient absorption changes in absorbance-matched solutions of TAPo and C_{60}, containing each 200 μM Car, are used to determine the quantum yield of triplet formation of TAPo.

Photobleaching. A solution of TAPo in toluene (14.5 μM) was irradiated with laser pulses (355 nm, 17.4 mJ per pulse, repetition frequency of 10 Hz) for several periods of time, and the absorption spectrum was recorded after each series of pulses. From the loss of absorption, the apparent quantum yield of photobleaching was calculated as 2.0×10^{-4} (see Supporting Information).

Electrochemistry. The redox potentials of TAPo were determined by cyclic voltammetry. Figure 10 shows the cyclic voltammogram of TAPo in benzonitrile. The oxidation branch shows two quasi-reversible processes. The reduction branch also shows two processes, the first one (I) clearly irreversible. From the position of the peaks, the redox potentials are deduced and are collected in Table 1.

4. Discussion

Effect of Aza Substitution on the Singlet-State Properties. Tetra-aza substitution of the porphycene ring induces large bathochromic shifts, thus validating the hypothesis that aza substitution in the macrocycle core is a valid strategy to shift its absorption spectrum to the red. This is a desired feature for PDT photosensitizers because tissue is more transparent in that spectral region.[4] Comparison of the redox potentials of TAPo to those of TPPo (Table 1) shows that the effect is due more to destabilization of the HOMO orbital rather than stabilization of the LUMO. The effect is larger for TAPo[38] than for its tetrapropyl counterpart,[49] revealing a synergistic effect of introducing both aza and phenyl substituents on the porphycene

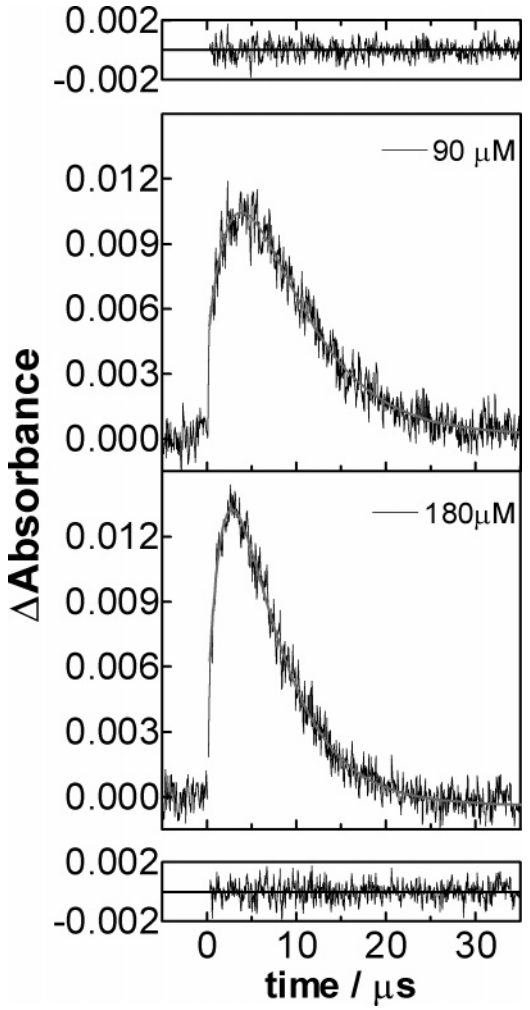

Figure 7. Transient absorption of the TAP−Car system in argon-saturated toluene ([TAP] = 90 μM; λ_{exc} = 662 nm, λ_{obs} = 524 nm), fit to a sum of two exponential functions, and residuals of the fit. Top: 90 μM Car; τ_1 = 3.8 μs, τ_2 = 8.0 μs. Bottom: 180 μM Car; τ_1 = 2.1 μs, τ_2 = 5.3 μs.

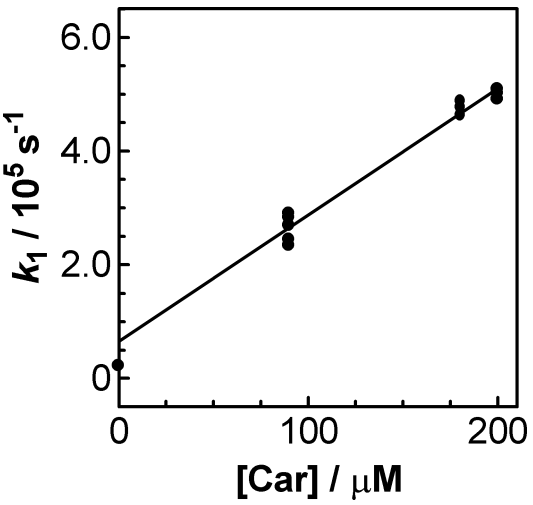

Figure 8. Effect of [Car] on the pseudo-first-order rate constant for ^{3}Car formation. The slope of the line is the rate constant for energy transfer, k_{et}, from ^{3}TAPo to Car.

ring (Figure 11). To check whether electronic communication between the phenyl rings and the macrocycle are responsible for this effect, the properties of the newly synthesized MTAPo were measured. Electronic communication is very unlikely in

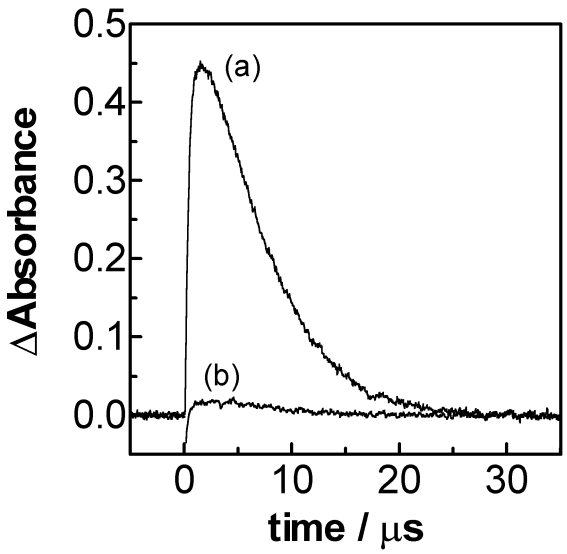

Figure 9. Absorbance changes in absorbance-matched deaerated solutions of (a) C_{60} and (b) TAPo 90 μM containing each [Car] = 200 μM in argon-saturated toluene. Samples were excited at 620 nm and the transients were observed at 524 nm. The transients could be fitted by a sum of two exponential functions, yielding τ_1 = 2.1 μs and τ_2 = 5.3 μs for TAPo, and τ_1 = 850 ns and τ_2 = 5.3 μs for C_{60}.

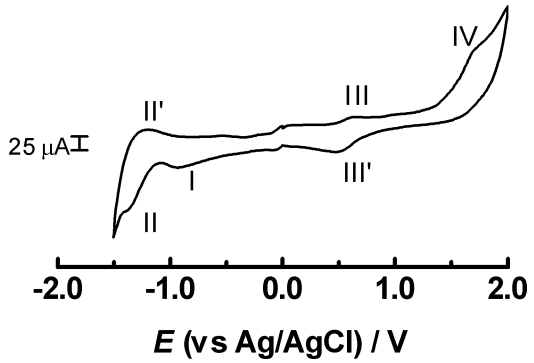

Figure 10. Cyclic voltammogram of TAPo (100 μM), in 0.1 M $TBAPF_6$ benzonitrile. Sweep speed: 100 mV·s^{-1}.

TABLE 1: Half-Wave Redox Potentials of TAPo in Benzonitrile (in V vs Ag/AgCl 3.5 M)[a]

	oxidation		reduction	
	first	second	first	second
TAPo	0.56	1.74	−0.92	−1.29
TPPo	1.12	-	−0.69	−0.94

[a] Values for TPPo in methylene chloride are given for comparison.[20] *E* vs Ag/AgCl 3.5 M in benzonitrile.

MTAPo because of the steric hindrance introduced by the *o*-methoxy group in the phenyl rings, which forces them out of the macrocycle plane. The noticeable blue shift in the absorption spectrum of MTAPo, as compared to that of TAPo, suggests that such electronic communication exists. Experiments are currently underway to better understand this effect.

The shape of the ground-state absorption spectrum of TAPo shows marked differences relative to those of TPPo.[20] The three Q-bands are less resolved and their relative intensities follow a clearly different pattern (Figure 1). Likewise, the Soret band is less intense. Interestingly, the differences are less obvious in the tetrapropyl series,[32,49] which, again, points to a synergistic effect between aza and phenyl substitution.

The fluorescence quantum yield and the singlet lifetime (Figure 2) are markedly lower than those of TPPo. This decrease

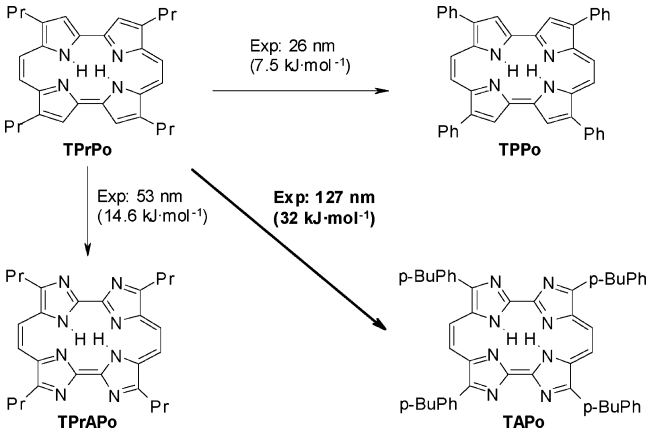

Figure 11. Effect of phenyl and aza substitution on the position of the lowest-energy absorption band of porphycenes. Introduction of four nitrogen atoms in the porphycene core causes a bathochromic shift of 53 nm.[32,49] Introduction of four peripheral phenyl substituents causes a shift of 26 nm. When the two modifications are simultaneously introduced, the total shift is 127 nm, larger than the sum of the individual effects.

is attributed to more efficient nonradiative decay pathways in TAPo, because the radiative rate constant is in fact larger for TAPo that for TPPo. Indeed, aza substitution causes a hyperchromic effect in the lowest-energy absorption band. Further insight into nonradiative processes is presented in the following sections.

Effect of Aza Susbstitution on the Triplet-State Properties. *Triplet Energy.* The introduction of four nitrogen atoms in the porphycene macrocycle also decreases the energy of its lowest triplet state, as determined from the phosphorescence spectrum (Figure 5). The decrease matches that observed in the singlet excited state, leading to similar singlet−triplet splittings in tetraazaporphycenes relative to porphycenes (59 kJ·mol^{-1} in TAPo vs 57 kJ·mol^{-1} in TPPo).

An independent determination of the triplet-energy value was obtained by energy-transfer experiments to β-carotene. When ^{3}TAPo is compared to $^3C_{60}$ as a triplet donor, two significant differences are observed (Figures 7 and 9): the rate constant for energy transfer is ca. 3-fold smaller and the lifetime of the resulting ^{3}Car shows a marked dependence on the concentration of Car.

These observations can be accounted for using the kinetic model shown in Scheme 1,[11,44−47,50,51] based on the monomer−excimer equilibrium treated originally by Birks.[52]

As shown in the Supporting Information, reversible energy transfer between a triplet donor and an acceptor results in biexponential absorbance changes:

$$\Delta A(t) = a_1 \exp(-k_1 t) + a_2 \exp(-k_2 t) \qquad (2)$$

where the convention has been adopted that k_1 is the largest rate constant and k_2 the smallest (see Figure 7).

k_1 in eq 2 is related to the forward- and reverse-energy-transfer rate constants k_{et} and k_{-et} by means of

$$k_1 = k_{et}[\mathrm{Car}] + k_{-et}[\mathrm{TAPo}] \qquad (3)$$

Hence, the variation of k_1 with [Car] at constant [TAPo] allows the determination of k_{et}. This dependence is shown in Figure 8, where k_{et} is the slope of the linear plot, i.e., $k_{et} = (2.2 \pm 0.2) \times 10^9$ M^{-1}·s^{-1}. Likewise, the intercept of the plot, $k_0 = (6.5 \pm 0.4) \times 10^4$ s^{-1}, combined with [TAPo] = 90 μM, yields $k_{-et} = (7.2 \pm 0.5) \times 10^8$ M^{-1}·s^{-1}. Ultimately, the two rate constants

SCHEME 1: Kinetic Models Used To Analyze the Energy Transfer from a Triplet Donor to β-Carotene[a]

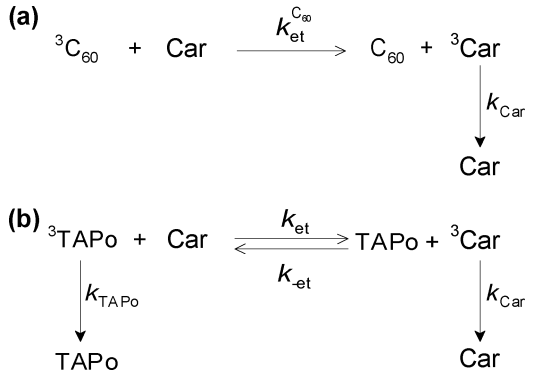

[a] Triplet donors were (a) C_{60}, (b) TAPo. $k_{et}^{C_{60}}$ is the rate constant for energy transfer from $^3C_{60}$; k_{car}, k_{TAPo} are the intrinsic rate constants for ^{3}Car and ^{3}TAPo decay, respectively; k_{et} and k_{-et} are the rate constants for direct and reverse energy transfer between ^{3}TAPo and ^{3}Car.

combine to yield the equilibrium constant for reversible energy transfer, $K_{et} = k_{et}/k_{-et} = 3.0 \pm 0.4$. Under the assumption that the conversion from ground to triplet state is devoid of any significant entropy changes,[47] eq 4 can be used to estimate the triplet energy of TAPo:

$$RT \ln K_{et} = -\Delta G_{et}^0 \approx E_{^3\mathrm{TAPo}} - E_{^3\mathrm{Car}} \qquad (4)$$

Using $E_{^3\mathrm{Car}} = 95$ kJ·mol^{-1} for Car as energy acceptor,[53,54] eq 4 sets the triplet energy of TAPo at 98 ± 2 kJ·mol^{-1}, in excellent agreement with the phosphorescence results.

Triplet Absorption Coefficient. As shown in the Supporting Information, the preexponential factors in eq 2 are related to the triplet-minus-singlet absorption coefficients of TAPo and Car, $\Delta\epsilon_{TAP}$ and $\Delta\epsilon_{Car}$, respectively, and can be used to determine $\Delta\epsilon_{TAP}$:

$$\Delta\epsilon_{\mathrm{TAPo}} = \Delta\epsilon_{\mathrm{Car}} \frac{(a_1 + a_2)k_{et}[\mathrm{Car}]}{a_2(p - k_2) - a_1(k_1 - p)} \qquad (5)$$

where p and q are defined in

$$p = k_{\mathrm{TAPo}} + k_{et}[\mathrm{Car}] \qquad q = k_{\mathrm{Car}} + k_{-et}[\mathrm{TAPo}] \quad (6)$$

Using the kinetic data in Figure 7, as well as the values for the different rate constants given in the preceding sections and $\Delta\epsilon = 1.01 \times 10^5$ M^{-1}·cm^{-1} at 524 nm,[55] the triplet-minus-singlet absorption coefficient of TAPo is calculated as $\Delta\epsilon = (1.7 \pm 0.7) \times 10^4$ M^{-1}·cm^{-1} at 524 nm (Figure 3).

Triplet Quantum Yield. The triplet quantum yield of TAPo was determined from transient absorption data by comparing the a_2 coefficients for absorbance-matched solutions of TAPo and C_{60} containing each [Car] = 200 μM (eq 7, see Supporting Information):

$$\Phi_T^{\mathrm{TAPo}} = \Phi_T^{C_{60}} \frac{a_2^{\mathrm{TAPo}}}{a_2^{C_{60}}} \frac{k_{et}^{C_{60}}[\mathrm{Car}]}{k_{et}^{C_{60}}[\mathrm{Car}] - k_{\mathrm{Car}}} \times \frac{(k_1 - k_2)\Delta\epsilon_{\mathrm{Car}}}{\Delta\epsilon_{\mathrm{TAPo}}(k_1 - p) + \Delta\epsilon_{\mathrm{Car}} k_{et}[\mathrm{Car}]} \qquad (7)$$

The results of this experiment are shown in Figure 9. Taking $\Phi_T^{C_{60}} = 1$,[56,57] the value of Φ_T for TAPo obtained by this method is 0.045 ± 0.005, in excellent agreement with the Φ_Δ value at high oxygen concentration.

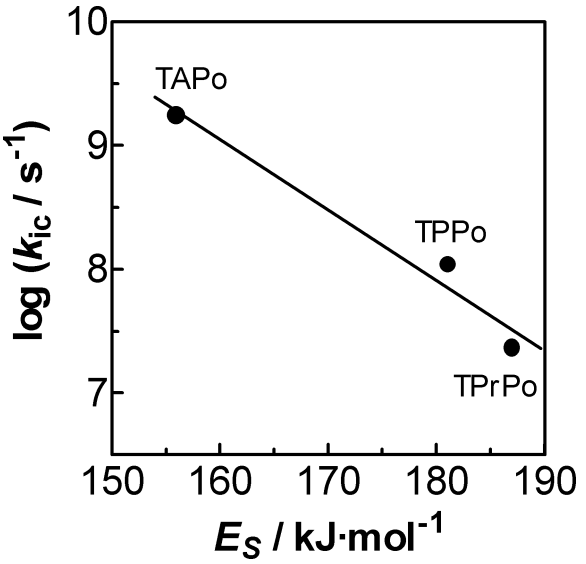

Figure 12. Correlation between the rate constant for internal conversion, k_{ic} and the sensitizer's singlet energy E_s for porphycenes[20,59] and tetraazaporphycene (this work).

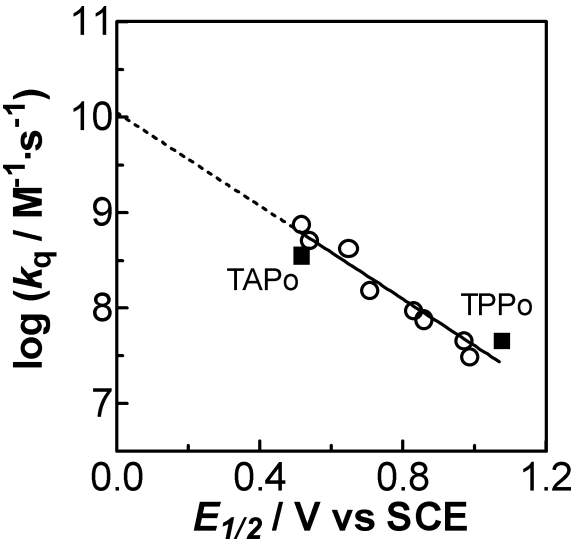

Figure 13. Correlation between the rate constant for quenching of $O_2(^1\Delta_g)$ by the sensitizer and the oxidation half-wave potential for porphyrinoid macrocycles,[62] and for TPPo and TAPo.

The triplet quantum yield is rather low and indeed much lower than that of TPPo ($\Phi_T = 0.33$).[20] The rate constant for $S_1 \rightarrow T_1$ intersystem crossing, $k_{isc} = \Phi_T/\tau_S = (8.7 \pm 0.7) \times 10^7\ s^{-1}$, is comparable to that of TPPo ($k_{isc} = 7.2 \times 10^7\ s^{-1}$), consistent with a similar singlet−triplet splitting in the two compounds. It must be concluded that internal conversion is the most efficient singlet decay pathway in TAPo, $\Phi_{IC} = 1 - \Phi_T - \Phi_F = 0.93$. For comparison, $\Phi_{IC} = 0.52$ in TPPo. Indeed, the rate constant for internal conversion, $k_{ic} = \Phi_{IC}/\tau_S = 1.8 \times 10^9\ s^{-1}$, is 15-fold larger than that of TPPo ($k_{ic} = 1.1 \times 10^8\ s^{-1}$).[20] The large increase in k_{ic} is likely the result of the energy-gap law, as suggested by the correlation between k_{ic} and the singlet energy E_s shown in Figure 12. This good linear correlation seems to indicate that porphycenes and azaporphycenes share a common dominant accepting vibrational mode.[58]

Singlet Oxygen Photosensitization. A sensitizer's triplet energy too close to or even below that of $O_2(^1\Delta_g)$ may lead to reversible energy transfer to this cytotoxic species.[44−47,60] This seems to be the case for TAPo, as suggested by the observations of (i) biexponential ^{3}TAPo decay kinetics in air-saturated solutions (Figure 4), (ii) a lower rate constant for oxygen quenching of the triplet state, and (iii) the strong variation of Φ_Δ with oxygen concentration (Figure 6). The possibility that oxygen enhances the quantum yield of ^{3}TAPo formation must be ruled out because the singlet lifetime is not affected by oxygen bubbling. Likewise, inefficient trapping of the triplet state by oxygen in air-saturated samples must also be ruled out given its natural lifetime of 44 μs, a quenching rate constant of $1.7 \times 10^9\ M^{-1}\cdot s^{-1}$, and an oxygen concentration in the millimolar range.

Although the triplet energy of TAPo is well above that of singlet oxygen, it must be taken into account that only one-ninth of the intervening collision complexes are of overall singlet multiplicity. This spin statistical factor effectively reduces the driving force for energy transfer,[44] $\Delta G_{et} \approx E^1_{O_2} - E^{3}_{TAPo} + RT \ln 9 = 1.6\ kJ\cdot mol^{-1}$, which results in an equilibrium constant of $K_{et} = 0.52$, consistent with the observations above. Overall, our singlet oxygen results parallel those observed for phthalocyanines with the same triplet energy.[61]

The rate constant for quenching of singlet oxygen by TAPo, $3.5 \times 10^8\ M^{-1}\cdot s^{-1}$, is higher than that observed for TPPo ($4.0 \times 10^7\ M^{-1}\cdot s^{-1}$).[20] Tanielian et al.[62] revealed a correlation between the quenching rate constant and the redox potentials for the oxidation of a group of chlorophylls and related porphyrinoids. As shown in Figure 13, TAPo falls very well on Tanielian's correlation, which suggests that charge transfer is the main mechanism of $O_2(^1\Delta_g)$ quenching by TAPo.

The apparent photobleaching quantum yield for TAPo, $\Phi_{-TAPo} = 2.0 \times 10^{-4}$ at 15.4 μM, is higher than that of related PDT photosensitizers:[63] haematoporphyrin, 4.7×10^{-5} (100 mM $NaHPO_4$, 0.22mM O_2); Photofrin, 5.4×10^{-5} (100 mM $NaHPO_4$, 0.22 mM O_2), Al(III) sulfonated phthalocyanine, 1.7×10^{-6} (H_2O) and lower than for chlorin e_6, 1.9×10^{-3} (100 mM $NaHPO_4$, 0.22 mM O_2) and Al(III) sulfonated naphthalocyanine, 3.0×10^{-3} (5% H_2O in MetOH). Assuming that reaction with singlet oxygen is the main contribution to photobleaching, eq 8 can be used to derive a more meaningful parameter, namely the rate constant for reaction of $O_2(^1\Delta_g)$ with TAPo:[64]

$$\Phi_{-TAPo} = \Phi_\Delta \frac{k_r[TAPo]}{1/\tau_\Delta^0 + k_q^{TAPo}[TAPo]} \qquad (8)$$

A value of $k_r = 2.4 \times 10^7\ M^{-1}\cdot s^{-1}$ is derived. This value is consistent with the low redox potential for the oxidation of TAPo and is comparable to that of porphyrinoids with a similar redox potential.[65]

5. Conclusions

2,7,12,17-Tetrakis(*p*-substituted phenyl)-3,6,13,16-tetraazaporphycenes are a novel class of porphyrinoid macrocycles. They were primarily designed as a new family of PDT photosensitizers based on the porphycene skeleton, aiming at shifting the absorption spectrum into the near-infrared where light penetration into tissue is optimal, and at increasing the absorption coefficient. Both goals are fulfilled by the compounds presented in this work. Compared to porphycenes, the tetraaza counterparts show stronger absorption in the near-infrared, lower-lying singlet and triplet excited states, and substantially larger internal conversion quantum yield ($\Phi_{IC} = 0.93$). The latter is mainly the result of the energy-gap law. Energy transfer to oxygen is observed, which results in the formation of the cytotoxic species singlet oxygen. The process is found to be reversible, consistent with a triplet-energy value close to that

of singlet oxygen. Although this challenges their use as therapeutic agents for PDT, it may be an advantage for other processes, e.g., diagnostics. The results of our studies provide clues for improving the design of novel photosensitizers based on the porphycene macrocycle.

Acknowledgment. This work was supported by the Spanish Programa Nacional de Biomedicina (MEC, SAF2002-0434-C02-02). N.R., O.R., and D.S.-G. thank the Fundació Patronat Institut Químic de Sarrià for their predoctoral fellowships. A.J.-B. thanks the Generalitat de Catalunya (DURSI) for a predoctoral fellowship as well.

Supporting Information Available: Synthesis of MTAPo and ETAPo. Beer−Lambert plots of TAPo. Absorption spectrum of MTAPo in benzene and of ETAPo in methanol and in water. Fluorescence decay of MTAPo. Fluorescence spectrum of MTAPo. Fluorescence quantum yield of TAPo and MTAPo. Quenching of triplet state of TAPo by oxygen. Triplet decay of TAPo at 1% oxygen concentration. Fi-delta of MTAPo. Irreversible energy transfer from $^3C_{60}$ to ^{3}Car. Photobleaching. Solution of the reversible energy transfer kinetic model. Relationship between the preexponential factors and the triplet-minus-singlet absorption coefficients. Relationship between the preexponential factors and the triplet quantum yields. This material is available free of charge via the Internet at http://pubs.acs.org.

References and Notes

(1) Spikes, J. D. *Photochem. Photobiol.* **1986**, *43*, 691.
(2) Rosenthal, I. A. *Photochem. Photobiol.* **1991**, *53*, 859.
(3) Montforts, F.-P.; Meier, A.; Scheurich, G.; Haake, G.; Bats, J. W. *Angew. Chem., Int. Ed. Engl.* **1992**, *31*, 1592.
(4) Jori, G. *J. Photochem. Photobiol. A: Chem.* **1992**, *62*, 371.
(5) Vallès, M. A. *Afinidad* **1993**, *50*, 469.
(6) Bonnett, R. *Chem. Soc. Rev.* **1995**, 19.
(7) Sternberg, E. D.; Dolphin, D.; Brückner, C. *Tetrahedron* **1998**, *54*, 4151.
(8) Allen, C. M.; Sharman, W. M.; Van Lier, J. E. *J. Porphyrins Phthalocyanines* **2001**, *5*, 161.
(9) Bonnett, R. *J. Heterocycl. Chem.* **2002**, *39*, 455.
(10) Arad, O.; Gavaldà, A.; Rey, O.; Rubio, N.; Sánchez-García, D.; Borrell, J. I.; Teixidó, J.; Nonell, S.; Cañete, M.; Juarranz, A.; Villanueva, A.; Stockert, J. C.; Díaz-Jiménez, P. J. *Afinidad* **2002**, *59*, 343.
(11) Mártire, D. O.; Jux, N.; Aramendía, P. F.; Negri, R. M.; Lex, J.; Braslavsky, S. E.; Schaffner, K.; Vogel, E. *J. Am. Chem. Soc.* **1992**, *114*, 9969.
(12) Xie, L. Y.; Boyle, R. W.; Dolphin, D. *J. Am. Chem. Soc.* **1996**, *118*, 4853.
(13) Sessler, J. L.; Weghorn, S. J. *Expanded, Contracted & Isomeric Porphyrins*, *Tetrahedron Organic Chemistry Series Volume 15*; Baldwin, J. E., Magnus, P. D., Eds.; Elsevier Science: Oxford, U.K., 1997.
(14) Bauer, V. J.; Clive, D. L. J.; Dolphin, D.; Paine, J. B.; Harris, F. L.; King, M. M.; Loder, J.; Wang, S. W. C.; Woodward, R. B. *J. Am. Chem. Soc.* **1983**, *105*, 6429.
(15) Jasat, A.; Dolphin, D. *Chem. Rev.* **1997**, *97*, 2267.
(16) Sessler, J. L.; Tvermoes, N. A.; Davis, J.; Anzenbacher Jr., P.; Jursíková, K.; Sato, W.; Seideel, D.; Lynch, V.; Black, C. B.; Try, A.; Andrioletti, B.; Hemmi, G.; Mody, T. D.; Magda, D. J.; Král, V. *Pure Appl. Chem.* **1999**, *71*, 2009.
(17) Sessler, J. L.; Seidel, D. *Angew. Chem., Int. Ed. Engl.* **2003**, *42*, 5134.
(18) Vogel, E.; Köcher, M.; Lex, J.; Ermer, O. *Isr. J. Chem.* **1989**, *29*, 257.
(19) Kudrevich, S. V.; Van Lier, J. E. *Coord. Chem. Rev.* **1996**, *156*, 163.
(20) Rubio, N.; Prat, F.; Bou, N.; Borrell, J. I.; Teixidó, J.; Villanueva, A.; Juarranz, A.; Cañete, M.; Stockert, J. C.; Nonell, S. *New J. Chem.* **2005**, *2*, 378.
(21) Montforts, F.-P.; Gerlach, B. *Tetrahedron Lett.* **1992**, *33*, 1985.
(22) Schiwon, K.; Brauer, H. D.; Gerlach, B.; Müller, C. M.; Montforts, F. P. *J. Photochem. Photobiol. B: Biol.* **1994**, *23*, 239.
(23) Singh, J. P.; Xie, L. Y.; Dolphin, D. *Tetrahedron Lett.* **1995**, *36*, 1567.
(24) Gerlach, B.; Montforts, F.-P. *Liebigs Ann.* **1995**, 1509.
(25) Kai, M.; Suzuki, M.; Masaki, Y. *Tetrahedron Lett.* **1998**, *39*, 4063.
(26) Nussbaumer, T.; Krieger, C.; Neidlein, R. *Eur. J. Org. Chem.* **2000**, *13*, 2449.
(27) Bonnett, R. *Chemical Aspects of Photodynamic Therapy*; Phillips, D.; O'Brien, P., Roberts, W. G., Eds.; Gordon and Breach Science Publishers: Amsterdam, **2000**.
(28) Braun, C. L.; Smirnov, S. N. *J. Chem. Educ.* **1993**, *70*, 612.
(29) Schweitzer, C.; Schmidt, R. *Chem. Rev.* **2003**, *103*, 1685.
(30) Jusélius, J.; Sundholm, D. *Phys. Chem. Chem. Phys.* **2000**, *2*, 2145.
(31) Vogel, E.; Köcher, M.; Schmickler, H.; Lex, J. *Angew. Chem., Int. Ed. Engl.* **1986**, *25*, 257.
(32) Aramendía, P. F.; Redmond, R. W.; Nonell, S.; Schuster, W.; Braslavsky, S. E.; Schaffner, K.; Vogel, E. *Photochem. Photobiol.* **1986**, *44*, 555.
(33) Nonell, S.; Bou, N.; Borrell, J. I.; Teixidó, J.; Villanueva, A.; Juarranz, A.; Cañete, M. *Tetrahedron Lett.* **1995**, *36*, 3405.
(34) Villanueva, A.; Cañete, M.; Nonell, S.; Borrell, J. I.; Teixidó, J.; Juarranz, A. *Anti-Cancer Drug Design* **1996**, *11*, 89.
(35) Cañete, M.; Lapeña, M.; Juarranz, A.; Vendrell, V.; Borrell, J. I.; Teixidó, J.; Nonell, S.; Villanueva, A. *Anti-Cancer Drug Design* **1997**, *12*, 543.
(36) Cañete, M.; Ortiz, A.; Juarranz, A.; Villanueva, A.; Nonell, S.; Borrell, J. I.; Teixidó, J.; Stockert, J. C. *Anti-Cancer Drug Design* **2000**, *15*, 143.
(37) Cañete, M.; Ortega, C.; Gavaldà, A.; Cristóbal, J.; Juarranz, A.; Nonell, S.; Teixidó, J.; Borrell, J. I.; Villanueva, A.; Rello, S.; Stockert, J. C. *Int. J. Oncol.* **2004**, *24*, 1221.
(38) Nonell, S.; Borrell, J. I.; Borrós, S.; Colominas, C.; Rey, O.; Rubio, N.; Sánchez-García, D.; Teixidó, J. *Eur. J. Org. Chem.* **2003**, *9*, 1635.
(39) Nonell, S.; Braslavsky, S. E. Time-resolved singlet oxygen detection. In *Singlet oxygen, UV-A, and Ozone. Methods in Enzymology*, *vol.319*, Packer, L., Sies, H., Eds.; Academic Press: San Diego, 2000; pp 37−49.
(40) Benson, R. C.; Kues, H. A. *J. Chem. Eng. Data* **1977**, *22*, 379.
(41) Oliveros, E.; Suardi-Muraseco, P.; Aminian-Saghafi, T.; Braun, A. M.; Hansen, H.-J. *Helv. Chim. Acta* **1991**, *74*, 79.
(42) Waluk, J.; Müller, M.; Swiderek, P.; Köcher, M.; Vogel, E.; Hohlneicher, G.; Michl, J. *J. Am. Chem. Soc.* **1991**, *113*, 5511.
(43) *Phthalocyanines: Properties and Applications*; Leznoff, C., Lever, A. B. P., Eds.; VCH Publishers: New York, 1989; Vols. 1−4.
(44) Firey, P. A.; Ford, W. E.; Sounik, J. R.; Kenney, M. E.; Rodgers, M. A. J. *J. Am. Chem. Soc.* **1988**, *110*, 7626.
(45) Rihter, B. D.; Kenney, M. E.; Ford, W. E.; Rodgers, M. A. J. *J. Am. Chem. Soc.* **1990**, *112*, 8064.
(46) Aoudia, M.; Cheng, G.; Kennedy, V. O.; Kenney, M. E.; Rodgers, M. A. J. *J. Am. Chem. Soc.* **1997**, *119*, 6029.
(47) Pelliccioli, A. P.; Henbest, K.; Kwag, G.; Carvagno, T. R.; Kenney, M. E.; Rodgers, M. A. J. *J. Phys. Chem. A* **2001**, *105*, 1757.
(48) Sasaki, Y.; Fujitsuka, M.; Watanabe, A.; Ito, O. *J. Chem. Soc., Faraday Trans* **1997**, *93*, 4275.
(49) Sargent, A. L.; Hawkins, I. C.; Allen, W. E.; Liu, H.; Sessler, J. L.; Fowler, C. J. *Chem. Eur. J.* **2003**, *9*, 3065.
(50) Kane-Maguire, N. A. P.; Toney, C. G.; Swiger, B. *Inorg. Chim. Acta* **1977**, *22*, L11.
(51) Kirk, A. D.; Navasivayam, C. *J. Phys. Chem.* **1989**, *93*, 5488.
(52) Birks, J. B. *Photophysics of Aromatic Molecules*; Wiley-Interscience: London, 1970; p 301.
(53) Herkstroeter, W. G. *J. Am. Chem. Soc.* **1975**, *97*, 4161.
(54) Schmidt, R. *J. Phys. Chem. A* **2004**, *108*, 5509.
(55) Nielsen, B. R.; Jørgensen, K.; Skibsted, L. H. *J. Photochem. Photobiol. A: Chem.* **1998**, *112*, 127.
(56) Arbogast, J. W.; Darmanyan, A. P.; Foote, C. S.; Rubin, Y.; Diederich, F. N.; Alvarez, M. M.; Anz, S. J.; Whetten, R. L. *J. Phys. Chem.* **1991**, *95*, 11.
(57) Hung, R. R.; Grabowski, J. J. *J. Phys. Chem.* **1991**, *95*, 6073.
(58) Englman, R.; Jortner, J. *Mol. Phys.* **1970**, *18*, 145.
(59) Nonell, S.; Aramendía, P. F.; Heihoff, K.; Negri, R. M.; Braslavsky, S. E. *J. Phys. Chem.* **1990**, *94*, 5879.
(60) Firey, P. A.; Rodgers, M. A. J. *Photochem. Photobiol.* **1987**, *45*, 535.
(61) Foley, S.; Jones, G.; Liuzzi, R.; McGarvey, D. J.; Perry, M. H.; Truscott, T. G. *J. Chem. Soc., Perkin Trans. 2* **1997**, 1725.
(62) Tanielian, C.; Wolff, C. *Photochem. Photobiol.* **1988**, *78*, 277.
(63) Spikes, J. D. *Photochem. Photobiol.* **1992**, *55*, 797.
(64) *Active Oxygen in Chemistry*; Foote, C. S., Valentine, J. S., Greenberg, A., Liebman, J. F., Eds.; Blackie Academic and Professional: Glasgow, 1995.
(65) Krasnovskii, A. A.; Veneditov, Y. A.; Chernenko, D. M. *Biophysics* **1982**, *27*, 1009.